

T. Syuto · N. Fujisawa · T. Takasugi ·  
T. Yamagata

## Flow visualization and scanning PIV measurement of three-dimensional structure in near field of strongly buoyant jet

Received: 9 May 2009/Accepted: 27 January 2010/Published online: 14 March 2010  
© The Visualization Society of Japan 2010

**Abstract** The near-field structure of strongly buoyant jet issuing from a square nozzle at low Froude and Reynolds numbers is studied by using LIF flow visualization and time-resolved scanning PIV. These experimental techniques allow the visualization of unsteady three-dimensional flow phenomenon occurring in the near-field of strongly buoyant jet. It is found that the buoyant jet is unstable to the positive buoyancy forces, which promote the inflow motion near the nozzle exit. The surrounding low temperature fluid moves into the nozzle inside along the nozzle corner and mixes with the high temperature fluid deep into the nozzle. Then, the flow pattern inside the nozzle becomes highly complex to promote the laminar to turbulent transition of the jet. The statistical flow characteristics of the strongly buoyant jet are evaluated from the scanning PIV measurement, and the result indicates the presence of axisymmetric distributions of mean flow and velocity fluctuations in the circle of diameter equal to the square side of the nozzle.

**Keywords** Flow visualization · Three-dimensional flow · Buoyant jet · LIF · Scanning PIV · Turbulence

### 1 Introduction

The buoyant flows are of great importance in many engineering problems related to fluid and thermal sciences. Examples of buoyant flows are observed in some atmospheric environments, such as spreading of smoke from chimney and drain, and in industrial flow-problems of pollution. The buoyant jet is termed by the buoyancy dominated flow issuing from a nozzle with a certain magnitude of momentum flux. Therefore, the fluid motion of buoyant jet is governed by inertial, buoyant and viscous forces, which are often characterized by source Froude and Reynolds numbers.

The classical works on buoyant jet are mostly concerned with the experimental studies on mean flow characteristics of the jets. The preliminary results on this subject are summarized by Chen and Rodi (1980) and List (1982), but most of them are concerned with the mean flow characteristics of fully developed region. Among these basic studies, some special attentions are placed on the stability and the laminar to turbulent transition of the buoyant jets by Anwar (1972), Mollendorf and Gebhart (1973), Ungate et al. (1975) and Pasumarthi and Agrawal (2005). The laminar buoyant jet is destabilized by the growth of asymmetric disturbances. The laminar length of the jet is studied experimentally at some combinations of the source Froude numbers and Reynolds numbers (Mollendorf and Gebhart 1973; Subbarao and Cantwell 1992). Later, turbulence measurements in the buoyant jets are reported by George et al. (1977), Papanicolaou and List (1988), Murota et al. (1989), Shabbir and George (1994), Dai et al. (1994), who

measured the turbulence characteristics of velocities and temperatures, using point measurement techniques, such as laser Doppler velocimetry, hot wire/film, thermocouple and laser-induced fluorescence techniques.

More recently, the structure of buoyant jet is investigated by Tian and Roberts (2003), Funatani et al. (2004) and Fujisawa et al. (2008) using LIF and PIV, and studied by Zhou et al. (2001) and Zhou and Hitt (2004) using large-eddy simulation. These results indicate that the structure of velocity and temperature field of the buoyant jet is dominated by asymmetrical modes of turbulence, which agrees with the result of the stability analysis by Mollendorf and Gebhart (1973). However, most of the previous studies are focused on the fully developed buoyant jet, so that there is very few knowledge about the near-field structure of buoyant jets. It should be mentioned that the experimental studies of buoyant jet in literature have been carried out using two-dimensional measuring techniques of LIF and PIV. Therefore, the three-dimensional structure has not been understood enough. In order to overcome this difficulty, the scanning PIV technique, which is one of the newly developed experimental techniques for three-dimensional flow, is introduced in the present study to explore the three-dimensional structure of buoyant jet. Note that this technique has been successfully applied to the studies of cold jet by Hori and Sakakibara (2004) and thermal convection by Fujisawa et al. (2005), but has not been applied to buoyant jet.

The purpose of this paper is to study the near-field flow characteristics of strongly buoyant jet at low Froude and Reynolds numbers issuing from a square nozzle, using flow visualization and scanning PIV for three-dimensional flow. A special attention is placed on the three-dimensional inflow motion inside the nozzle, which has not been studied in literature.

## 2 Experimental methods

### 2.1 Experimental apparatus

The three-dimensional flow visualization and velocity measurement of strongly buoyant jet are carried out using an experimental apparatus as shown in Fig. 1. The volume of the test tank is  $400 \times 400 \times 400 \text{ mm}^3$ , which is filled with cold water. The hot water is supplied into the test tank through the bottom square hole having  $d = 20 \text{ mm}$  in side length. A large volume of hot water is prepared in a separate tank with temperature controller, and is supplied to the test tank through the long straight square pipe of 470 mm in length, which is connected to the bottom hole of the test tank. Note that the straight pipe is insulated by Styrofoam. The buoyant jet is generated from the bottom hole of the test tank and is diffused into the stagnant cold water environment. The temperature of hot water is measured by a thermocouple placed in the settling chamber, which is placed just upstream of the straight pipe, while the bulk velocity of the buoyant jet is varied by using a valve and measured by a flow meter. In the present study, experiments are carried out at hot water temperatures ranging from 10 to 25°C and at cold water temperature 10°C. The bulk velocity through the pipe is varied in the range from 8.9 to 13.1 mm/s to keep a constant Reynolds number  $Re (= V_0 d / v) = 200$ , where  $V_0$  mean velocity at nozzle exit,  $v$  kinematic viscosity of hot water. Therefore, the

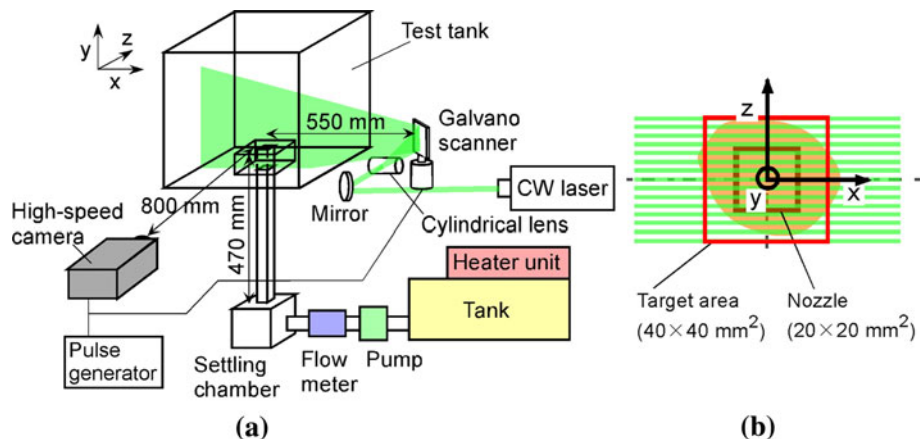


**Fig. 1** Experimental apparatus for flow visualization and PIV measurement. **a** Experimental apparatus, **b** top view around nozzle exit

source Froude number  $Fr_0$  ( $= V_0 / \sqrt{dg(\rho_c - \rho_h)/\rho_h}$ ) is ranged from  $\infty$  to 0.39, where  $g$  gravitational acceleration,  $\rho$  density of fluid, and subscripts c and h denote cold and hot state. In this study, LIF flow visualization and scanning PIV measurement are applied to investigate near-field structure of strongly buoyant jet. The target area is -20 to 20 mm in  $x$  direction, -45 to 45 mm in  $y$  direction, and -20 to 20 mm in  $z$  direction, which covers the near-field of strongly buoyant jet including the flow inside the nozzle.

## 2.2 Flow visualization

The flow visualization is carried out using the fluorescent dye solution (Rhodamine B) illuminated by a CW Nd:YAG laser of 5 W (Watanabe et al. 2005). In the present study, the light sheet is traversed quickly using a scanner system, which consists of Galvano scanner, mirror and controller as described in Fig. 1. This scanner system is located at 550 mm apart from the target flow to provide planar light sheets at various  $z$  positions almost parallel to each other. Note that the maximum deflection angle of the light sheet is 2°.

The time chart of scanning system is illustrated in Fig. 2. According to this diagram, the planar light sheet moves linearly from the original position ( $z = -20$  mm) to the other end of the target space ( $z = 20$  mm) during the period of 15 ms. After this scanning motion, the light sheet moves back quickly to the original position in 2 ms. The scanning mode is repeated at every 0.2 s to capture 1,000 images. The synchronous observation is made by a high speed CCD camera combined with a pulse controller. The CCD camera operates at 2,000 frames/s during the imaging and captures 30 images in a cycle of positive scanning motion. The captured images have spatial resolutions of 1,280 × 1,024 pixels with 8 bits in gray level.

## 2.3 Three-dimensional scanning PIV

The periodic illumination and observation using the scanning system in combination with the high speed CCD camera allows the PIV measurement of three-dimensional velocity field of strongly buoyant jet. For this purpose, the flow field is visualized by nylon tracer particles, which are 80  $\mu\text{m}$  in diameter with relative density of 1.02. In order to improve the traceability of the particles, the density of working fluid is controlled by adding small amount of salt. The particle size was determined from the condition of high accuracy in PIV measurement, which corresponds to about 2 pixels in the pixel images.

The time chart of scanning PIV measurement is shown in Fig. 2. By scanning the light sheet in  $z$  direction during the period of 15 ms, 15 frames of image are captured by the high speed CCD camera operating at 1,000 frames/s. This is followed by the negative scanning motion of 2 ms. The scanning mode is repeated in the next 17 ms to capture a sequential two images for PIV measurement. This mode was repeated at every 0.2 s to capture 1,000 sets of images. It should be mentioned that the slower frame rate of imaging in the scanning PIV than that of the LIF flow visualization is due to the lower scattering light from the tracer particles in comparison with the LIF flow visualization. The PIV analysis is applied to the sequential two images of the first and second scanning motion at the same  $z$  position. Note that the time interval of the two images is 17 ms. Then, the planar velocity field at each cross-sections of the buoyant jet

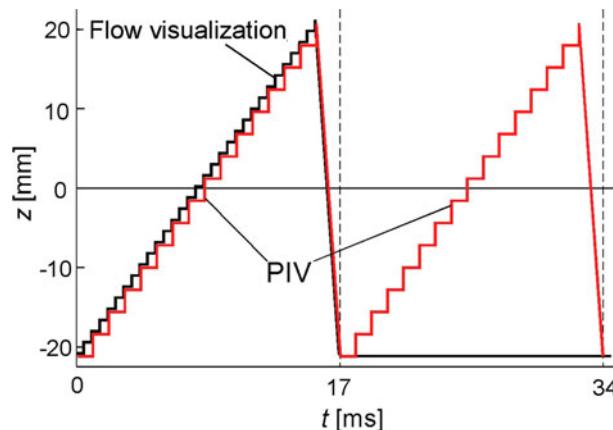


**Fig. 2** Time chart of scanning light sheet

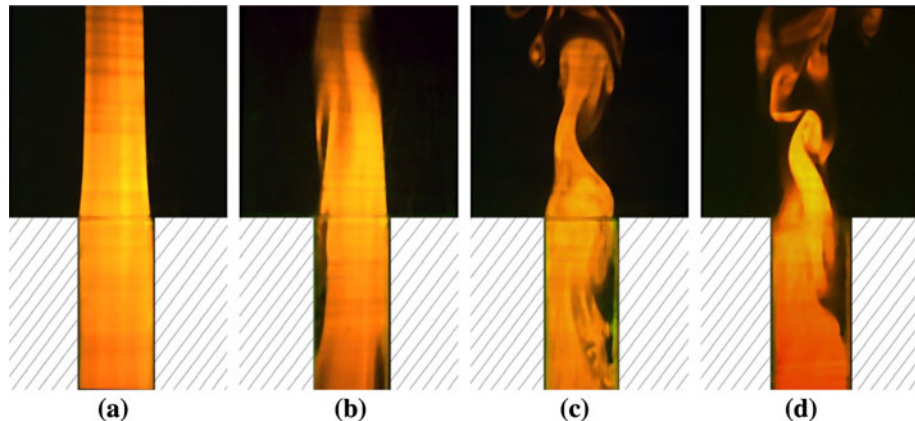
is evaluated from the cross-correlation algorithm with sub-pixel analysis. The interrogation window size is set to  $31 \times 31$  pixels and the search window size is  $41 \times 41$  pixels. The tracer particles are observed about 2 pixels and the maximum particle displacement is approximately 10 pixels, which allows the appearance of error vectors  $<1\%$  of the total number of analyzed velocity vectors. The accuracy of velocity measurement is estimated as 3% with uncertainty interval of 95%. When the time scale of the target flow is much larger than the scanning time period, the three-dimensional velocity field is almost frozen (Hori and Sakakibara 2004; Fujisawa et al. 2005). This is the case of the present strongly buoyant jet at low Froude and Reynolds numbers.

### 3 Results and discussion

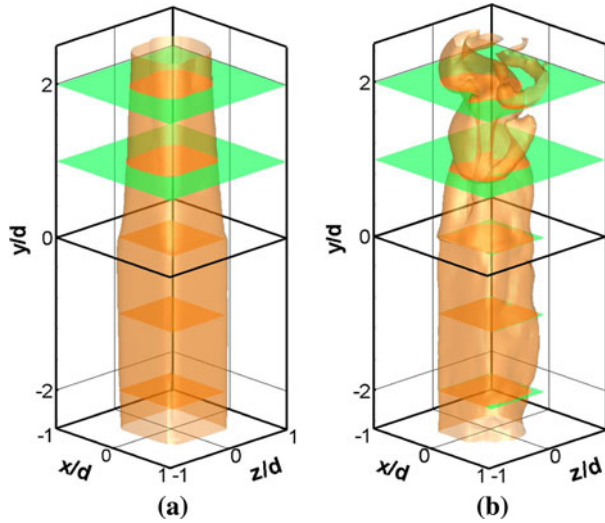
#### 3.1 Flow visualization of buoyant jet

Figure 3 shows examples of flow visualization pictures taken at some source Froude numbers  $Fr_0 = \infty$ , 1.05, 0.58, 0.39 and at Reynolds number  $Re = 200$ . The flow observations are made by a standard color CCD camera operated at 30 frames/s, and the observations are made at the central planar section ( $x$ - $y$  plane) of the square nozzle. The flow visualization picture for non-buoyant jet (Fig. 3a) indicates the development of the laminar jet upward without any roll-up motion. Note that weird straight line at the nozzle exit is due to the effect of light reflection of the laser at the interface of acrylic material surrounding the nozzle. When the source Froude number decreases slightly to 0.92, the jet flow is accelerated by the buoyancy force and the flow becomes unstable near the nozzle exit, which results in a roll-up motion of the buoyant jet as shown in Fig. 3b. Note that the inflow motion is observed near the right hand corner of the square nozzle. With further decrease in source Froude number to 0.58 (Fig. 3c) and 0.39 (Fig. 3d), the flow becomes more unstable and the roll-up motion is promoted to appear in a shorter distance from the nozzle exit. Although the jet flow behaves turbulent in the far region of the nozzle, there exists small laminar region in and outside the nozzle exit. Therefore, such flow state is considered as unsteady. It should be mentioned that unsteady nature of the flow is caused by the buoyancy-induced flow near the nozzle exit, which is shown by the dark area in the nozzle.

Figure 4a, b shows the three-dimensional flow visualizations of the non-buoyant jet ( $Fr_0 = \infty$ ) and buoyant jet ( $Fr_0 = 0.58$ ), respectively, which are investigated at  $Re = 200$ . These results are obtained from the scanning laser sheet technique in the present study combined with the volumetric rendering technique. These three-dimensional visualizations give more clear view of flow structure than those of two-dimensional visualizations. The cross-sectional views and the three-dimensional contours of non-buoyant and buoyant jets are well observed in the three-dimensional visualizations. The visualization for non-buoyant jet shows the development of laminar flow even in the outside of the nozzle. Only the change of the flow structure can be seen in the cross-sectional shape of the jet in the outside of the nozzle. On the other hand, the flow visualization result for buoyant jet indicates the presence of vortical nature of the flow in the far region from the nozzle, which seems to be triggered by the flow inside the nozzle. The inflow motion is found near the



**Fig. 3** Examples of LIF flow visualization of buoyant jet. **a**  $Fr_0 = \infty$ , **b**  $Fr_0 = 1.05$ , **c**  $Fr_0 = 0.58$ , **d**  $Fr_0 = 0.39$



**Fig. 4** Three-dimensional reconstruction of LIF flow visualization for non-buoyant and buoyant jet. **a** Non-buoyant jet ( $Fr_0 = \infty$ ), **b** buoyant jet ( $Fr_0 = 0.58$ )

exit of the square corner of the nozzle and penetrates deep into the nozzle to promote the laminar to turbulent transition of the flow inside the nozzle.

### 3.2 Instantaneous velocity field of buoyant jet

Figures 5 and 6 show the instantaneous velocity vectors and the vertical velocities  $v/V_0$  of the buoyant jet reconstructed from the scanning PIV measurement of buoyant jet at  $Fr_0 = 0.58$ ,  $Re = 200$ . Figure 5 is the velocity contours at some vertical cross-sections of the buoyant jet. The results indicate that the vertical velocity becomes large even outside the nozzle exit, which is due to the acceleration of the jet velocity by buoyancy forces. It should be mentioned that the inflow velocity appears near the corner of the square nozzle, and it penetrates into the nozzle as deep as two to three times of the nozzle side length. The inflow velocity distribution is found to be asymmetrical near the nozzle, which corresponds to the swaying growth of the buoyant jet in vertical direction along the side surface of the nozzle. The deflection of the buoyant jet seems to be large as it approaches the nozzle exit. Figure 6 shows the corresponding instantaneous velocity field at some horizontal planes. These results confirm that the inflow velocity is found along the corner of the

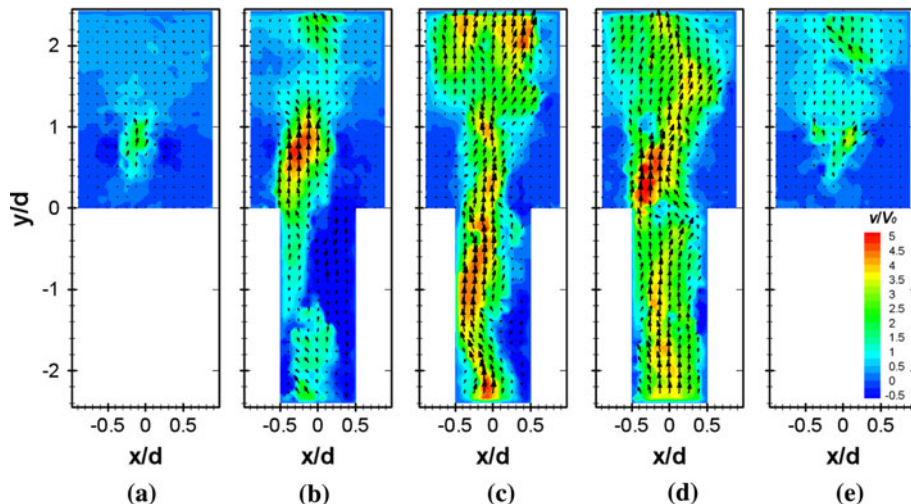


**Fig. 5** Instantaneous velocities of buoyant jet in vertical plane. **a**  $z/d = -0.6$ , **b**  $z/d = -0.3$ , **c**  $z/d = 0$ , **d**  $z/d = 0.3$ , **e**  $z/d = 0.6$

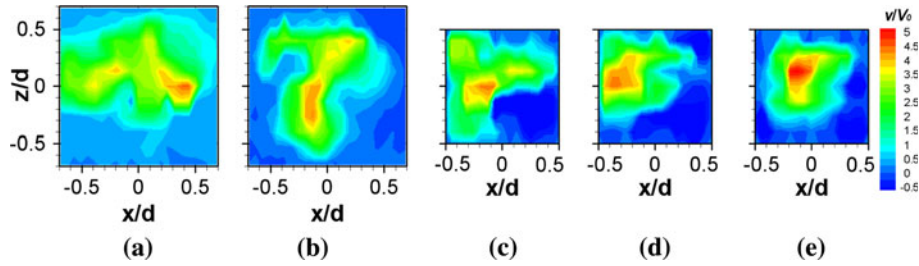


**Fig. 6** Instantaneous velocities of buoyant jet in horizontal plane. **a**  $y/d = 2$ , **b**  $y/d = 1$ , **c**  $y/d = 0$ , **d**  $y/d = -1$ , **e**  $y/d = -2$

square nozzle, and the jet flow develops along the nozzle deflecting in side direction. It is also found that the maximum velocity of the buoyant jet shows high peaks even in the outside of the nozzle, and the jet width spreads in horizontal direction.

### 3.3 Mean flow and fluctuating velocity characteristics

The three-dimensional mean velocity field of the buoyant jet is evaluated from 1,000 sets of instantaneous velocity fields obtained from the scanning PIV measurement. The results are shown in Figs. 7 and 8, which corresponds to the vertical and horizontal slices of the three-dimensional velocity field, respectively. Each figure shows the mean velocity vectors and vertical mean velocities  $V/V_0$ . These results indicate that the high temperature fluid moves along the nozzle surface upward and it grows in width as the vertical distance increases, as was expected from the instantaneous velocity fields. The inflow velocity is found near the corner of the square nozzle and it reaches up to 40% of the mean velocity  $V_0$  of the buoyant jet. As the horizontal velocity contour in Fig. 8 is almost circular independent of the vertical distance, the mean

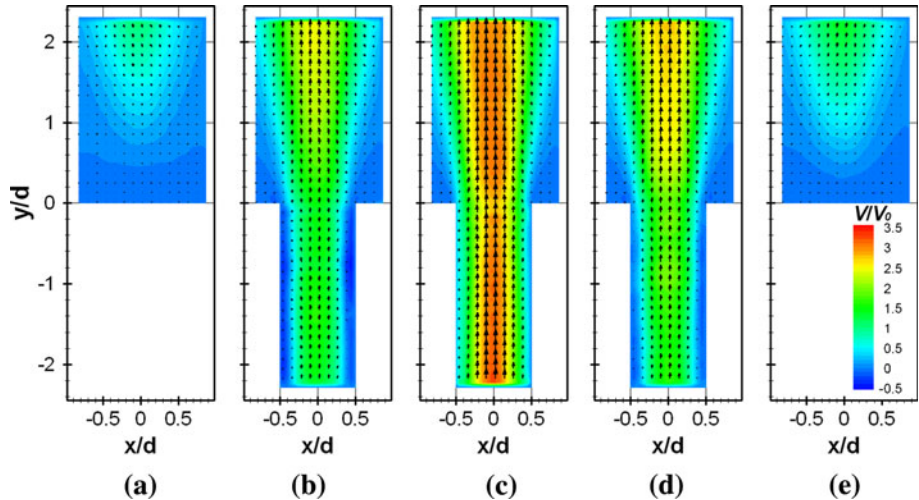


**Fig. 7** Mean velocities of buoyant jet in vertical plane. **a**  $z/d = -0.6$ , **b**  $z/d = -0.3$ , **c**  $z/d = 0$ , **d**  $z/d = 0.3$ , **e**  $z/d = 0.6$

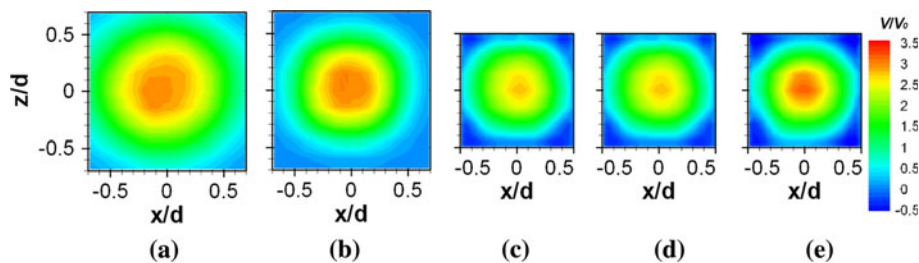


**Fig. 8** Mean velocities of buoyant jet in horizontal plane. **a**  $y/d = 2$ , **b**  $y/d = 1$ , **c**  $y/d = 0$ , **d**  $y/d = -1$ , **e**  $y/d = -2$

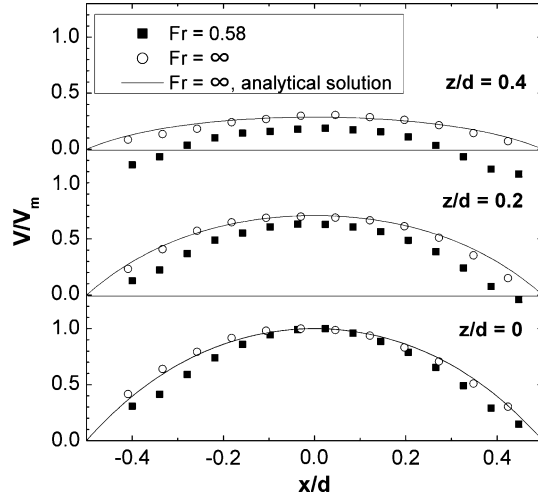
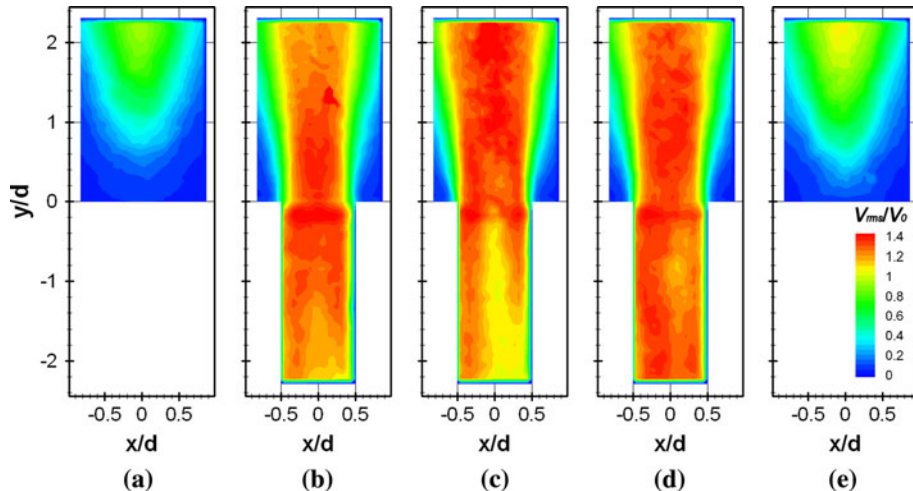


**Fig. 9** Mean velocity distributions  $V/V_m$  inside nozzle ( $y/d = -1$ )

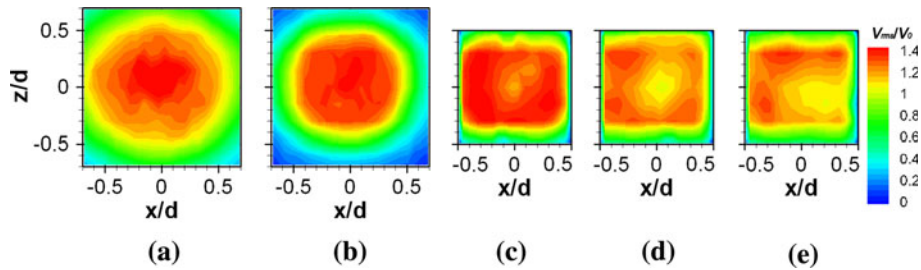
velocity field is considered axisymmetric distributions in the circle of diameter equal to the square side of the nozzle. Thus, the mean inflow velocity occurs at four corners of the square nozzle, while the jet flow develops along the nozzle upward by attaching the side surface of the nozzle.

Figure 9 shows the mean velocity distributions in horizontal plane of the buoyant jet at some positions of  $z/d = 0, 0.2$  and  $0.4$  inside the nozzle ( $y/d = -1$ ), which are compared with the counterparts of non-buoyant jet. Note that the mean velocity distributions are normalized by the centerline velocity  $V_m$  for comparative purposes. The mean velocity distributions at the centerline ( $z/d = 0$ ) shows a laminar profile for both non-buoyant and buoyant jet. Note that the velocity profile of non-buoyant jet agrees closely with the analytical profile for laminar square duct (Knudsen and Katz 1979). The velocity profile of buoyant jet shows slightly lower velocity magnitude in the off-center plane of  $x/d$ . When the target planes are shifted to  $z/d = 0.2$  and  $0.4$ , the deviations of velocity distributions are magnified between the non-buoyant and buoyant jet. It should be mentioned that the negative velocity was clearly observed in the buoyant jet at  $z/d = 0.4$  in the range of  $x/d > 0.3$  and  $x/d < -0.3$ , which corresponds to the region near the corner of the square nozzle. These results confirm that the inflow appears strongly near the corner of the square nozzle, which has been observed in the LIF flow visualization and scanning PIV measurement.

The velocity fluctuations of the buoyant jet are shown in Figs. 10 and 11, which correspond to the vertical and horizontal slices of the three-dimensional velocity fluctuation field, respectively. These results indicate that large velocity fluctuations are found outside the nozzle exit, but they are still observed inside



**Fig. 10** Fluctuating velocities of buoyant jet in vertical plane. **a**  $z/d = -0.6$ , **b**  $z/d = -0.3$ , **c**  $z/d = 0$ , **d**  $z/d = 0.3$ , **e**  $z/d = 0.6$



**Fig. 11** Fluctuating velocities of buoyant jet in horizontal plane. **a**  $y/d = 2$ , **b**  $y/d = 1$ , **c**  $y/d = 0$ , **d**  $y/d = -1$ , **e**  $y/d = -2$

the nozzle, too. The presence of large velocity fluctuations in the nozzle is expected to be due to the unsteady nature of the buoyant jet induced by the inflow motion of the surrounding cold fluid into the nozzle. They are distributed almost in a square shape along the inner surface of the nozzle and shifted to a circular shape as the flow develops in the outside of the nozzle, which suggests the presence of highly turbulent region in the inflow along the corner of the square nozzle.

#### 4 Conclusions

The LIF flow visualization and scanning PIV measurement are successfully applied to the study of three-dimensional flow field in the near-field of strongly buoyant jet at low Froude and Reynolds numbers. The flow visualization study indicates the occurrence of unstable inflow motion from the surrounding cold fluid into the nozzle through the square corner of the nozzle. This is due to the thermal instability of the buoyant jet at the interface of the hot and surrounding cold fluid. The instantaneous velocity contour measured by scanning PIV shows the presence of unsteady inflow velocity near the corner of the square nozzle, and the surrounding cold fluid penetrates into the hot fluid in the nozzle as deep as two to three times of the nozzle side length, which can promote the laminar turbulent transition of the buoyant jet. The mean velocity contour in the horizontal plane shows circular shape, which indicates axisymmetric nature of the mean velocity field. On the other hand, the fluctuating velocity contour in the horizontal plane shows square shape inside the nozzle and it shifts to a circular along the jet axis, which indicates the presence of large velocity fluctuations in the inflow.

#### References

- Anwar HO (1972) Appearance of unstable buoyant jet. *J Hydraul Div HY*7:1143–1156
- Chen CJ, Rodi W (1980) Vertical turbulent buoyant jets: a review of experimental data. Pergamon Press, Oxford
- Dai Z, Tseng L-K, Faeth GM (1994) Structure of round, fully developed, buoyant turbulent plumes. *J Heat Transf* 116:409–417
- Fujisawa N, Funatani S, Katoh N (2005) Scanning liquid-crystal thermometry and stereo velocimetry for simultaneous three-dimensional measurement of temperature and velocity field in a turbulent Rayleigh-Bernard convection. *Exp Fluids* 38:291–303
- Fujisawa N, Funatani S, Watanabe Y (2008) Simultaneous imaging techniques for temperature and velocity fields in thermal fluid flows. *J Vis* 11:247–255
- Funatani S, Fujisawa N, Ikeda H (2004) Simultaneous measurement of temperature and velocity using two-colour LIF combined with PIV with a colour CCD camera and its application to the turbulent buoyant plume. *Meas Sci Technol* 15:983–990
- George WK, Alpert RL, Tamanini F (1977) Turbulence measurements in an axisymmetric buoyant plume. *Int J Heat Mass Transf* 20:1145–1154
- Hori T, Sakakibara J (2004) High-speed scanning stereoscopic PIV for 3D vorticity measurement in liquids. *Meas Sci Technol* 15:1067–1078
- Knudsen JG, Katz DL (1979) Fluid dynamics and heat transfer. Krieger, New York, p 101
- List EJ (1982) Turbulent jets and plumes. *Ann Rev Fluid Mech* 14:189–212
- Mollendorf JC, Gebhart B (1973) An experimental and numerical study of the viscous stability of a round laminar vertical jet with and without thermal buoyancy for symmetric and asymmetric disturbances. *J Fluid Mech* 61:367–399
- Murota A, Nakatsuji K, Tamai M (1989) Experimental study on turbulence structure in turbulent plane forced plume. *J Jpn Soc Civ Eng* 405:79–87
- Papanicolaou PN, List EJ (1988) Investigations of round vertical turbulent buoyant jets. *J Fluid Mech* 195:341–391

- Pasumarthi KS, Agrawal AK (2005) Buoyancy effects on flow transition in low-density inertial gas jets. *Exp Fluids* 38:541–544
- Shabbir A, George WK (1994) Experiments on a round turbulent buoyant plume. *J Fluid Mech* 275:1–32
- Subbarao ER, Cantwell BJ (1992) Investigation of co-flowing buoyant jet: experiments on the effects of Reynolds number and Richardson number. *J Fluid Mech* 245:69–90
- Tian X, Roberts PJW (2003) A 3D LIF system for turbulent buoyant jet flows. *Exp Fluids* 35:636–647
- Ungate CD, Harleman DRF, Jirka GB (1975) Stability and mixing of submerged turbulent jets at low Reynolds numbers. Energy Laboratory Report MIT-EL 75-014
- Watanabe Y, Hashizume Y, Fujisawa N (2005) Simultaneous flow visualization and PIV measurement of turbulent buoyant plume. *J Vis* 8:293–294
- Zhou X, Hitt DL (2004) Proper orthogonal decomposition analysis of coherent structures in a transient buoyant jet. *J Turbul* 5:1–21
- Zhou X, Luo KH, Williams JJR (2001) Large eddy simulation of a turbulent forced plume. *Eur J Mech B/Fluids* 20:233–254